



# Numerical Simulation of Flow Separation Control using Multiple DBD Plasma Actuators

R. Khoshkhoo and A. Jahangirian<sup>†</sup>

*Aerospace Engineering Department, Amirkabir University of Technology, Tehran, Iran*

<sup>†</sup>*Corresponding Author Email: [ajahan@aut.ac.ir](mailto:ajahan@aut.ac.ir)*

(Received July 18, 2015; accepted August 22, 2015)

## ABSTRACT

A numerical simulation method is employed to investigate the effect of the steady multiple plasma body forces on the flow field of stalled NACA 0015 airfoil. The plasma body forces created by multiple Dielectric Barrier Discharge (DBD) actuators are modeled with a phenomenological plasma method coupled with 2-dimensional compressible turbulent flow equations. The body force distribution is assumed to vary linearly in the triangular region around the actuator. The equations are solved using dual-time implicit finite volume method on unstructured grids. In this paper, the responses of the separated flow field to the effects of single and multiple DBD actuators over the broad range of angles of attack ( $9^\circ - 30^\circ$ ) are studied. The effects of the actuators positions on the flow field are also investigated. It is shown that the DBD have a significant effect on flow separation control in low Reynolds number aerodynamics.

**Keywords:** Flow Control; Dielectric Barrier Discharge; Numerical Simulation; Multiple Plasma Body Forces; Low Reynolds Number Flow.

## 1. INTRODUCTION

Flow separation is an undesirable phenomenon which causes loss of lift force, increases drag force and produces control problems for different aerospace vehicles. The solution of this problem is thus highly demanded in fluid dynamics researches (Greenblatt and Wygnanski 2000).

Flow separation control can be achieved by active and passive methods. The DBD plasma actuator is one of the active flow control devices that have been successfully used in flow separation control applications. Thus, studies in this field have increased rapidly over the last decade (Corke *et al.* 2010, Tathiri *et al.* 2014).

The DBD actuator consists of two electrodes which are separated by a layer of dielectric material. The schematic of the actuator is shown in Fig. 1. The actuator operates in the frequency range of 1-50 KHz and voltage amplitude of 1-20 KV. If AC current is imposed on the two electrodes, the plasma forms on the dielectric layer beyond the exposed electrode. Plasma is accelerated from the right side of the exposed electrode due to the electric field between the two electrodes. Thus, plasma contacts the air molecules and the momentum of plasma is transferred to the flow inside the boundary layer. Induced flow (pseudo wall jet) is created which produces suction above the exposed electrode.

DBD operates in steady and unsteady mode. The unsteady mode in comparison with steady mode has lower input energy consumption. In this study, a DBD actuator in the operational steady mode is assumed.

First-principles-based modeling and phenomenological modeling are two approaches for simulation of the DBD plasma actuator. First-principles-based modeling approaches are very accurate in analysis of the interaction between the electric discharge and the near wall flow physics. Three classifications of this type of models are: kinetic models, fluid models and hybrid models. Priority in selection of these models is mainly based on the treatment of the plasma chemistry, environmental conditions and geometrical complexity (Jayaraman and Shyy2008). However, the main objective of the phenomenological modeling is the simulation of the plasma and their effects on the flow. They are simple to implement and computationally cheap. Therefore, they are used in different applications (Jayaraman and Shyy2008). The phenomenological approach in comparison with the first-principle-based modeling approach cannot definitely predict the plasma physics, but it is rather simple and very appropriate for simulation of the effects of plasma on the fluid. Full description about both approaches is presented by Jayaraman and Shyy (2008).

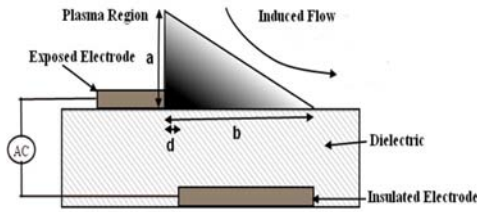


**Fig. 1. Diagram of a DBD plasma actuator and its effective region.**

The Shyy model is one of the well-known models from the phenomenological modeling approach that is employed in several two and three dimensional fluid dynamics problems (Visbal 2010; Gaitonde 2005, 2010; Jayaraman *et al.* 2007, Jayaraman and Shyy 2008; Shyy *et al.* 2002) and its results are compared with the experimental data in the study by Jayaraman and Shyy (2003). In this model, the effect of the plasma actuator on the fluid flow is assumed as a body force in the triangular region with the dimensions of  $a$  and  $b$  (see Fig. 1). The dimensions of  $a, b$  and  $d$  are 2.2 mm, 3mm and 0.25 mm respectively. In this region, the electric field is linearized and its lines are parallel except in the small region near the cathode. Additionally, as the distance from the cathode increases, the strength of the electric field lines decreases (Jayaraman and Shyy 2008). It should be noted that the results of the Shyy model are reported to be comparable with the experimental data in low flow velocities, frequency ranges of 1-7 KHz and voltage amplitudes of 1-10 KV (Jayaraman and Shyy 2003, Shyy *et al.* 2002).

Jayaraman *et al.* (2007) showed that multi-DBD actuators have a greater effect on the flow control than the single actuator, especially at a high angle of attack. Tsubakino and Tanaka (2007) also showed that the effect of using a single actuator with high Dc on the flow field is the same as two actuators of half Dc.

Therefore, the use of multi-DBD actuators has attracted much interest in the recent years. The usual multi-DBD actuators are bipolar multiple DBD and traditional multiple DBD actuators (Jiangnan *et al.* 2014). In the traditional type, upper and lower electrodes are isolated by dielectric and all DBDs are operated separately. In the bipolar type, the first upper and the last lower electrodes are isolated by dielectric and the other upper and lower electrodes are conducted by an electrical wire. More details in this regard are described in the study by Jiangnan *et al.* (2014). In this study, traditional multiple DBD actuators are assumed and the strength of the electric field (Dc) is similar for all actuators.

In fact, using single actuator with higher voltage has practical problems of requiring a more powerful AC generator and decreasing the efficiency and lifetime of the DBD plasma actuator. Therefore, using the multiple DBD actuators are increasingly required. However, a comprehensive study has not been done until now, especially with similar input electric power over the broad range of angles of

attack and different number of actuators.

The advantages of the DBD plasma actuator are very useful for Micro Air Vehicles (MAVs) or MARS airplane in which the aerodynamics performance is highly affected by the flow separation. MAVs operate under low Reynolds number ( $Re < 10^5$ ) flow conditions. Two and three dimensional simulations in this field are carried out by Gaitonde *et al.* (2005). They found that when the attachment process is complete and separation is completely inhibited, the 3-D simulation is essentially 2-D near the airfoil, with negligible computed span wise velocities in the vicinity of the airfoil, except downstream of the trailing edge. So it can be assumed that, all results in this study with 2D flow field assumption are similar to the corresponding 3-D results.

In the present study, the flow passing a stalled NACA0015 airfoil under the impact of plasma body force at low speed conditions is explored. The impact of the single and multiple DBD actuators and their locations over the flow field at various angles of attack is investigated.

## 2. COMPUTATIONAL METHOD

### 2.1 Governing flow Equations

Based on the acoustic measurements, it is reported that compressibility effects may play an important role in the momentum coupling process (Baird *et al.*, 2005), although the temperature of the air around DBD does not change considerably (Corke *et al.* 2005). Therefore, in this study, two-dimensional compressible Navier-Stokes equations are applied as the governing flow equations, which are augmented by source terms representing the plasma force of the DBD actuator. The flow equations can be written in general and non-dimensional form as follows:

$$\frac{\partial \rho^*}{\partial t^*} + \nabla^* \cdot (\rho^* \vec{U}^*) = 0 \quad (1)$$

$$\frac{\partial \rho^* \vec{U}^*}{\partial t^*} + \nabla^* \cdot (\rho^* \vec{U}^* \vec{U}^* + p^* \vec{I}) - \nabla^* \cdot \vec{\tau}^* = D_c q^* \vec{E}^* \quad (2)$$

$$\frac{\partial \rho^* e^*}{\partial t^*} + \nabla^* \cdot [(\rho^* e^* + p^*) \vec{U}^* - (\vec{U}^* \cdot \vec{\tau}^*) - Q_{ht}^*] = \beta D_c q^* \vec{U}^* \cdot \vec{E}^* \quad (3)$$

where non-dimensional quantities are denoted by superscript\*.  $\vec{U}^* = \{u^*, v^*\}$ ,  $\rho^*$ ,  $p^*$ ,  $t^*$ ,  $e^*$ ,  $\vec{I}$  and  $\vec{\tau}^*$  represent the velocity vector, density, pressure, time, total energy per unit value, unit vector and shear stress tensor, respectively.  $Q_{ht}^*$  is the heat conduction term. All mentioned values are non-dimensional based on the following scaling:

$$\rho^* = \frac{\rho}{\rho_{ref}}, U^* = \frac{U}{\frac{a_{ref}}{\sqrt{\gamma}}} = \frac{U}{\sqrt{\frac{p_{ref}}{\rho_{ref}}}}, p^* = \frac{p}{p_{ref}}, \quad (4)$$

$$e^* = \frac{e}{p_{ref}}, \mu^* = \frac{\mu}{\mu_{ref}} \frac{M \sqrt{\gamma}}{Re}, T^* = \frac{T}{T_{ref}}$$

where the subscript ref and superscript \* denote the reference and non-dimensional values, respectively.  $U, \mu, \gamma$  and  $a_{ref}$  represent the velocity vector, the molecular viscosity coefficient, ratio of specific heats and sound speed, respectively. Non-dimensional parameters  $Re$  and  $M$  denote the Reynolds number and the Mach number, respectively. The perfect gas is assumed, and the Sutherland law is used to calculate the molecular viscosity coefficient. In this study, the flow is assumed turbulent when the actuator is not active. The Algebraic Prandtl turbulence model is used for calculation of the flow. In this model, the eddy viscosity is derived from the following equation:

$$\mu_t = \rho L_m^2 \left| \frac{\partial u}{\partial y} \right| \quad (5)$$

Where  $\mu_t$  is the eddy viscosity,  $L_m$  is the mixing length and  $\frac{\partial u}{\partial y}$  is the local mean velocity gradient. The mixing length is given by:

$$L_m = \kappa y \left[ 1 - e^{-\frac{y^+}{A^+}} \right] \quad (6)$$

$\kappa, y, A^+$  and  $y^+$  are the Von Karman constant, the surface normal distance, constant (mostly equal to 26) and non-dimensional surface normal distance, respectively (Wilcox, 1998).

## 2.2 Plasma Actuator Modeling

In equations (2) and (3),  $D_c q^* \vec{E}^*$  and  $\beta D_c q^* \vec{U}^* \cdot \vec{E}^*$  are body force and energy induced by the plasma actuator on the fluid flow, respectively. Where  $\vec{E}^*$  is the electric field vector,  $q^*$  is the charge number density and  $\beta$  is the parameter either 0 or 1, which is used to show the effect of the energy produced and the work done by body force. Actually, the work done by plasma force is very small; so  $\beta$  is assumed to be zero in this study. More details in this regard are described in Gaitonde *et al.* (2005).  $D_c$  is the non-dimensional plasma force magnitude parameter, which is defined as:

$$D_c = \frac{\rho_{c,ref} e_c E_{ref} L_{ref}}{P_{ref}} \quad (7)$$

$e_c, \rho_{c,ref}, P$  and  $L$  denote the electronic charge (electrons), charge number density, pressure and the chord length, respectively.

In this study, the Shyy model is employed to simulate the effect of plasma force on the flow field. It is assumed that the plasma region is a triangular area down-stream the exposed electrode on the dielectric layer (see Fig. 1). The strength of the plasma body force depends on  $D_c$  and the size of the triangular area ( $a, b$  in Fig. 1). Plasma body force is assumed to be constant in the Shyy model with steady state assumption. Also, it is assumed that the extent of the electric field in the plasma region decreases linearly along with the direction axes.

In the present study the actuator operates in a steady mode. More details about the Shyy model are

described in Jayaraman and Shyy (2008) and Shyy *et al.* (2002). Also, the values of  $\theta = 3kHz, \rho_c = 10^{11}/cm^3, \Delta t = 67\mu s, \frac{a}{L} = 0.018, E_b = 30 kV/cm$  and  $\frac{b}{L} = 0.024$ , were adapted from the work of Gaitonde *et al.* (2005).

## 2.3 Numerical flow Solution Method

Two-dimensional compressible Navier-Stokes equations are applied as the governing flow equations. The Algebraic Prandtl turbulence model is used for turbulent flow simulation.

The flow field is unsteady and the mean values of the flow variables are obtained by averaging the instantaneous values over several time periods. A cell-center implicit finite-volume method is employed following the work of Jahangirian *et al.* (2005) to discretize the governing equations. The artificial dissipation terms are added to the main flow equations for numerical stability reasons. So semi-discrete form of the Navier-Stokes equations is represented as:

$$\frac{d}{dt}(Q_i A_i) + R_i(Q) - D_i(Q) = 0 \quad (8)$$

Where  $R_i(Q)$  denotes the convective and viscous fluxes,  $A_i$  is the area of the cell and  $D_i(Q)$  is the artificial dissipation flux. The artificial dissipation terms provide background dissipation to suppress odd-even modes using a blend of first and third-order dissipative terms.

In this study, residual smoothing and the explicit four stages Runge-Kutta method are applied. The CFL number of 50000 is used for the implicit algorithm and convergence to steady state error ( $10^{-6}$ ) is considered.

For viscous flows, no-slip boundary conditions were imposed. Non-reflecting boundary conditions are also used in the far-field based on the characteristic method (Jahangirian and Hadidoolabi 2005).

In this study, an unstructured grid is generated around NACA0015 airfoil, which is exhibited in Fig. 2. The outer boundary is situated about 15 chords from the airfoil. Actuators are located at 0.028 and 0.078 of the chord length. The number of points and cells of the grids for different combinations of actuators is presented in table 1. Grids are concentrated around the plasma actuator. In the neighborhood of the actuators 90 points are considered over the airfoil.

## 3. RESULTS AND DISCUSSION

Two cases are considered in this study. The first one is the flow over NACA0015 airfoil without-control actuator at 14 degrees angle of attack, Reynolds number 63000 and free-stream Mach number 0.2 in order to validate the numerical method. Results are compared with those of available experimental and numerical results (Asada and Fujii 2010).

In the second case, the DBD plasma actuator over

the same airfoil at Mach number 0.1 and Reynolds number 45000 based on the chord length is used and

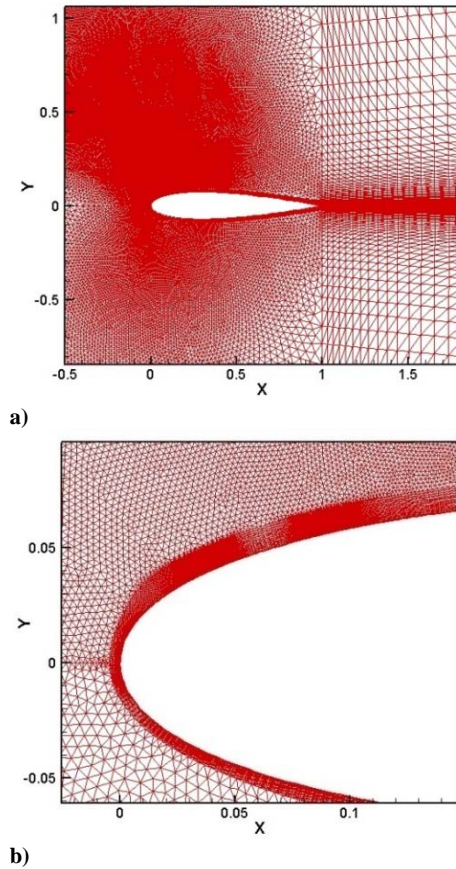


Fig. 2. Generated grid.

Table 1 The number of points and cells for each grid

Unstructured grid	The number of points	The number of cells	The number of points over airfoil surface
Without actuator	53946	107282	345
One actuator	63663	126676	385
Two actuators	88733	176726	475
Three actuators	128906	256962	585
Four actuators	180487	360005	704

The effects of using these stall control devices are studied. In all simulations, the Prandtl number is assumed 0.72 and the ratio of the specific heat is 1.4.

### 3.1 Flow Without-Control

The flow conditions for this case are  $\alpha = 14$ ,  $Re = 63000$  and  $M_\infty = 0.2$ . The nature of the flow at this high incidence angle is unsteady due to the large flow separation over the airfoil and shedding the wakes down-stream the airfoil. The mean surface

pressure coefficients ( $C_p$ ) are exhibited in Fig. 3. compared with the alternative numerical and experimental results (Asada and Fujii 2010; Kaneda *et al.* 2012). The mean surface friction coefficients ( $C_f$ ) are shown in Fig. 4 compared with the three-Dimensional LES numerical simulation results (Kaneda and Asada 2011). In this case the flow separation is initiated at approximately 2% of the chord length from the leading edge. More details can be found in Khoshkhoo and Jahangirian (2014).

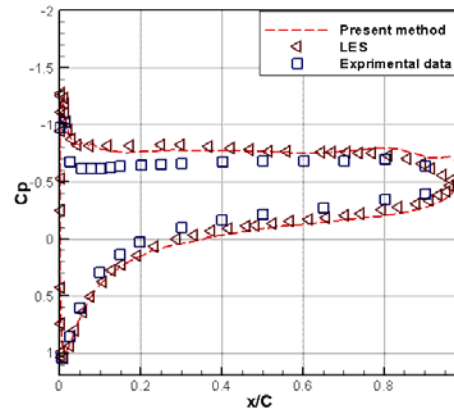


Fig. 3. Mean surface  $C_p$  distributions without control,  $M=0.2$ ,  $A.O.A=14$ .

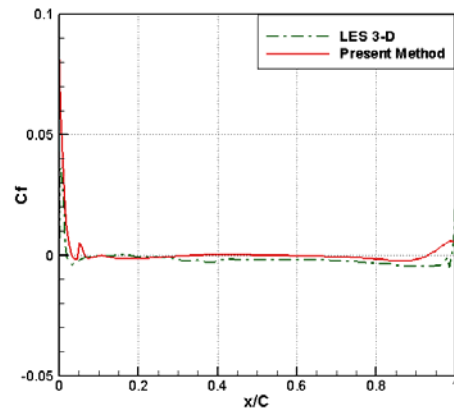


Fig. 4. Mean surface  $C_f$  distributions without control,  $M=0.2$ ,  $A.O.A=14$ .

### 3.2 The Effect of Single Plasma Actuator

In the second case there is a DBD plasma actuator which controlled the flow separation. To compare the results with the reference data (Gaitonde *et al.* 2005), the angle of attack was set at 15 degrees. Reynolds number and Mach number are 45000 and 0.1, respectively. In without-control condition; the separation is initiated at 2.4% of the chord length from the leading edge, which is compatible with those of the above reference and the result of Visbal (2010). The actuator is placed at 2.8% of the chord from the leading edge on the upper surface.  $D_c = 33.6$  is assumed. The mean surface pressure coefficient ( $C_p$ ) distribution as exhibited in

Fig.5 is compared with the two dimensional DNS results of Gaitonde (2005). As illustrated, the differences are small and in both results the flow is attached through the majority of the airfoil surface except for a small region near the trailing edge (see Fig.6).

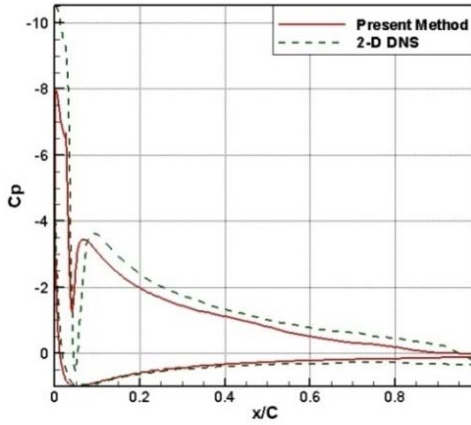


Fig. 5.  $C_p$  distributions with control at  $M=0.1, AOA=15$ .

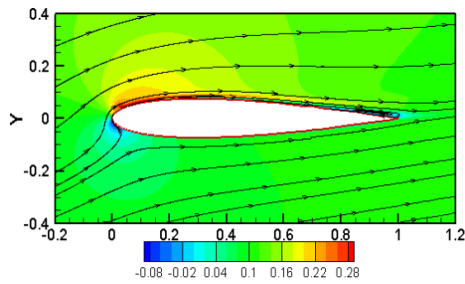


Fig. 6. Mean stream lines and U-velocity contours with one plasma actuator.

### 3.3 The Effect of Multiple Plasma Actuators

The flow separation control using two, three and four actuators is investigated in this section. In all cases, the first actuator is located at the 2.8% chord from the leading edge and other actuators are placed by distance of 5% of the chord from the previous actuators as shown in Fig.7. Also, it is assumed that the total strength of the multiple plasma actuators electric field ( $D_c$ ) is equal to the single actuator. For example, DBDs in two-actuators are placed at 2.8% and 7.8% of the chord from the leading edge.  $D_c = 16.8$  is assumed for each actuator which is half of the strength of the single actuator. The mean surface pressure coefficient ( $C_p$ ) distributions with multiple actuators are exhibited in Fig.8 in comparison with those of single actuator. It is visible that in all cases, flow separation exists in a small region near the trailing edge and the pressure gradient is observable close to every plasma actuator location. Stream line and mean U-velocity contours for the single and multiple actuators are shown in Fig.9. It is notable that, by increasing the number of

actuators while keeping the total  $D_c$  the separation area increases in the trailing edge. Also, the mean lift and drag coefficients for different composition of actuator(s) are shown in table 2.

The mean U-velocity profile at mid-chord position for the 15 degrees angle of attack is shown in figure 10. It is visible that by increasing the number of actuators the maximum u-velocity remains positive. It is interesting that the multiple actuators have a mean lift coefficient higher than the single actuator while keeping the total  $D_c$ . Also, the mean drag coefficient is smaller than the single actuator. Also, the two and three actuators cases have lift to drag coefficient ratios ( $\frac{C_l}{C_d}$ ) higher than others. Thus, the two and three actuators have better performance than the others. However, it can be seen that increasing the number of DBDs further to three actuators by decreasing the electric voltage does not seem to improve the aerodynamic performance.

It is concluded that the multiple actuators have a greater effect on the flow separation control with the same electrical power requirements.

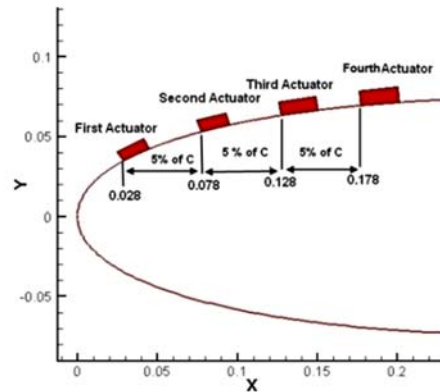


Fig. 7. Schematic of the actuator locations on the airfoil.

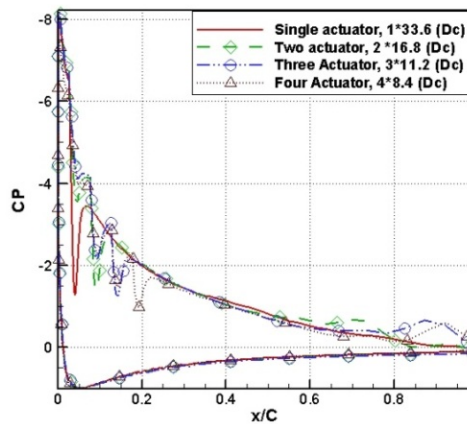


Fig. 8. Surface  $C_p$  distributions with one and multiple plasma actuator(s).

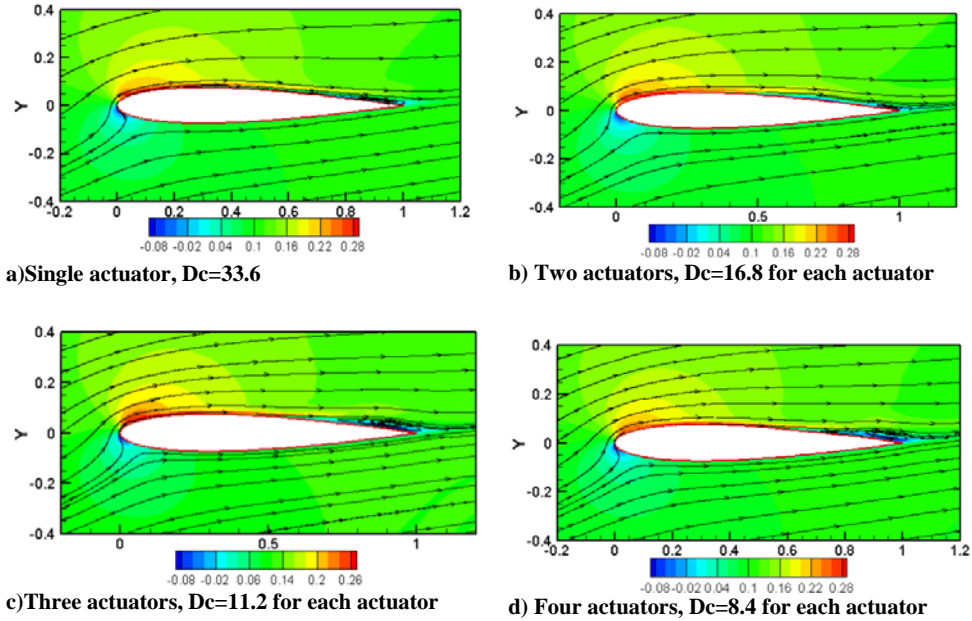


Fig. 9. Stream lines and mean U-velocity contours with different number of actuators,  $M=0.1$ ,  $A.O.A=15$ .

Table 2 The mean lift and drag coefficients

	$C_l$	$C_d$	$\frac{C_l}{C_d}$
Without actuator	0.5485	0.2212	2.4796
One actuator	1.5195	0.0761	19.9671
Two actuators	1.7168	0.0465	36.9204
Three actuators	1.7209	0.0684	25.1593
Four actuators	1.5749	0.0753	20.9150

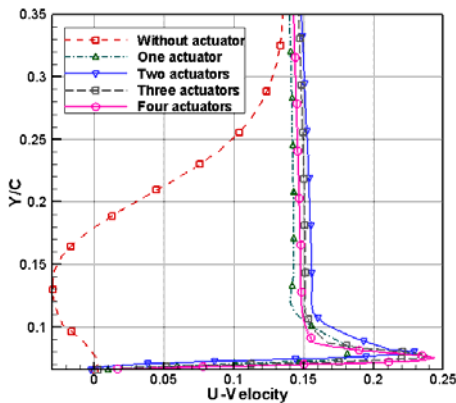


Fig. 10. Mean U-velocity profile in mid-chord.

### 3.4. The Effect of Plasma Actuators Location

It was concluded in the previous section that the use of multiple DBD actuators can improve the separation control. Thus, it is necessary to survey the effect of actuator location over the flow structure. First of all, a two actuator model is

considered and the effect of the second actuator location in separation control is studied. In all cases, the angle of attack of 15 degrees,  $M=0.1$  and  $Re=45000$  are assumed. The first actuator is located at 2.8% of the chord from the leading edge, which is close to the separation point. It is appropriate location to place the first actuator. More details can be found in Khoshkhoo and Jahangirian (2014). The second actuator is placed in different locations that are shown Fig. 11. The mean surface pressure coefficient ( $C_p$ ) distributions for the two actuators in different locations are shown in Figs. 12. It seems that by increasing the distance between two actuators, the flow separation control will increase. The mean streamline and u-velocity contours for all cases are exhibited in Fig. 13. It is shown that by increasing the distance between two actuators, flow separation lodges between two actuators, separation after the trailing edge disappears and maximum velocity decreases in the leading edge.

The mean lift and drag coefficients ( $C_l, C_d$ ) for different second actuator locations are visible in table 3. It is clear that the first and third cases have a maximum lift coefficient to drag coefficient ratios ( $\frac{C_l}{C_d}$ ) which are shown in Fig. 14. Minimizing the distance between the two actuators will improve the aerodynamic performance if their electric fields do not interact in such a short distance. It can be noted that placing the second actuator at a minimum distance of the first actuator and 0.3 of the chord length (about maximum thickness of airfoil) from the first actuator improves the aerodynamic performance coefficients. By increasing distance between actuators, the mean drag coefficients will increase and the mean lift coefficients will decrease.

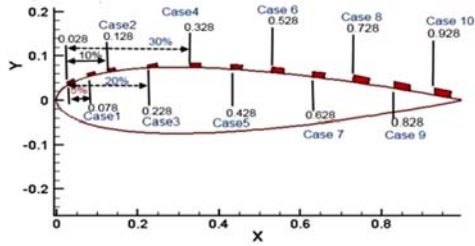
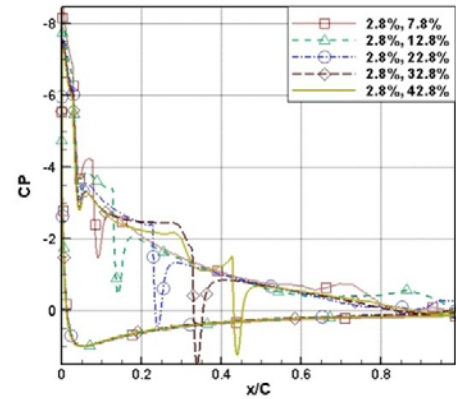
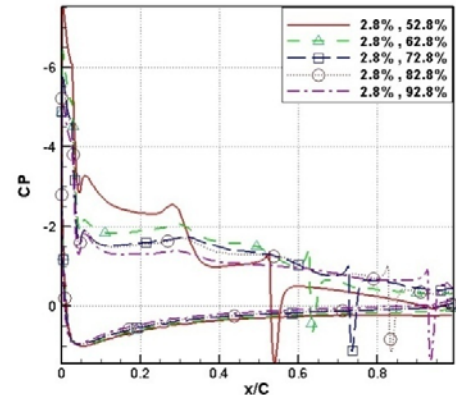


Fig. 11. Schematic of two actuators' location.



a)



b)

Fig. 12. Surface  $C_p$  distributions with different second actuator locations.

**- Triple Plasma Actuators**

The effect of the third and second actuator location in the three plasma actuators over flow structure in the three plasma actuators over flow structure is studied. In all cases, the angle of attack of 15 degrees,  $M=0.1$  and  $Re=45000$  are assumed. The first actuator is fixed and located at 2.8% of the chord length from the leading edge. To survey the effect of the second actuator over flow structure, it is placed at 5% and 10% of the chord length from the first actuator and the third actuator is placed at different positions that are shown in Fig. 15. The mean lift and drag coefficients of three actuators with the second actuator located at 5% of the chord

length from the first actuator are shown in table 4. Results show that the maximum of lift to drag coefficient ratios ( $\frac{C_l}{C_d}$ ) is achieved by locating the third actuator in 30-40% of the chord length from the leading edge (surrounding maximum thickness of airfoil) which is visible in Fig. 16. Also, placing the third actuator near the second actuator improve the aerodynamic performance coefficients in the second order. Particularly, the location of the third actuator affects the drag coefficient.

Table 3 The mean lift and drag coefficients

Case	The second actuator location from the first actuator	$C_l$	$C_d$	$\frac{C_l}{C_d}$
1	5% chord	1.7168	0.0465	36.9204
2	10% chord	1.6572	0.0602	27.5528
3	20% chord	1.5365	0.0509	30.1866
4	30% chord	1.5538	0.0558	27.8458
5	40% chord	1.5656	0.0736	21.2717
6	50% chord	1.6881	0.0913	18.4896
7	60% chord	1.6833	0.1975	8.52430
8	70% chord	1.5296	0.2007	7.6213
9	80% chord	1.4959	0.2073	7.2161
10	90% chord	1.2969	0.2107	6.1552

The mean surface pressure coefficient ( $C_p$ ) distribution for three actuators in different locations is shown in Fig. 17. Mean stream line and mean U-velocity contours for all cases are exhibited in Fig.18. It seems that by increasing the distance between the third and second actuator, flow separation lodges between the two actuators.

Results of three multiple actuators with the second actuator location in 10% of the chord from the first actuator show a decreasing distance between the first and second actuators, which can improve the aerodynamic coefficients.

**3.5. The Effect of Single and Multiple Plasma Actuator(s) in Various Angles of Attack**

The effects of the single and multi-DBD actuator(s) over the flow field in the broad range of angles of attack ( $9^\circ - 30^\circ$ ) are investigated. Summation of Dc in the multiple plasma actuators equal to 33.6.  $Re=45000$  and  $M=0.1$  are considered. The mean lift coefficients ( $C_l$ ) in various angles of attack are shown in table 5. In low angles of attack, the use of one actuator is more effective than others. In medium angles of attack (12-18 degrees), the use of two and three actuators is more effective than others and finally, in high angles of attack (above 18 degrees); four actuators have the greatest impact on flow control separation and increasing lift. The mean drag coefficients ( $C_d$ ) in various angles of

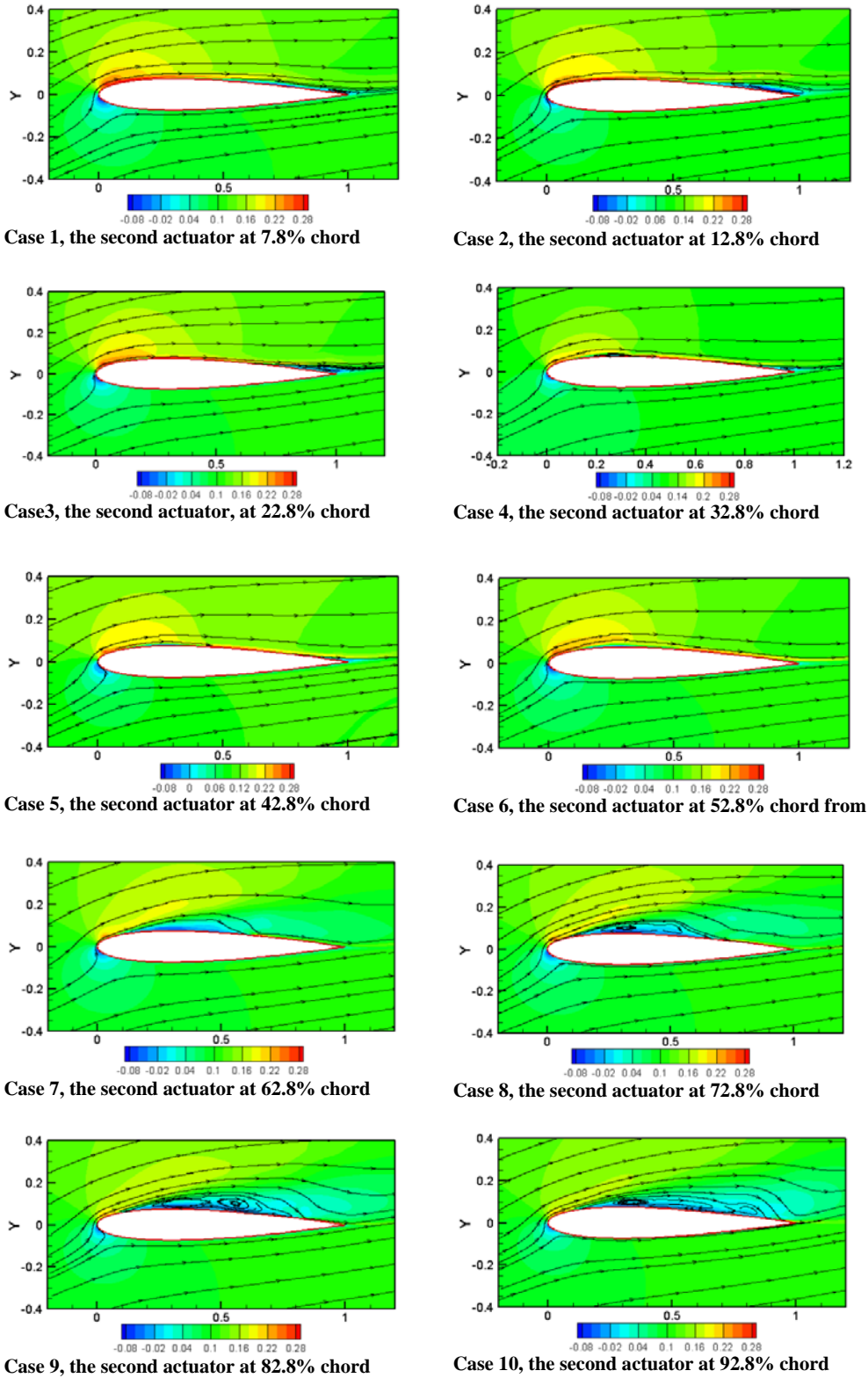


Fig. 13. Mean streamline and mean U-velocity contours with different locations of the second actuator.

attack are shown in Fig. 19. The results show that in low angles of attack, discrepancy between drag

coefficients is small and one actuator has the lowest  $C_d$ . By increasing the angle of attack, its

discrepancy increases and the multiple plasma actuators have lower drag coefficients. It is suggested that in low angles of attack, one actuator is used with maximum Dc. In medium angles of attack, two and three actuators are applied and in high angles of attack, four actuators are effective on the flow separation control. It seems that, on the condition that the DBD plasma actuators don't have interaction each other and input voltage greater than minimum voltage for ionized air surrounding actuator, by increasing number of actuators, the greater angles of attack can be controlled.

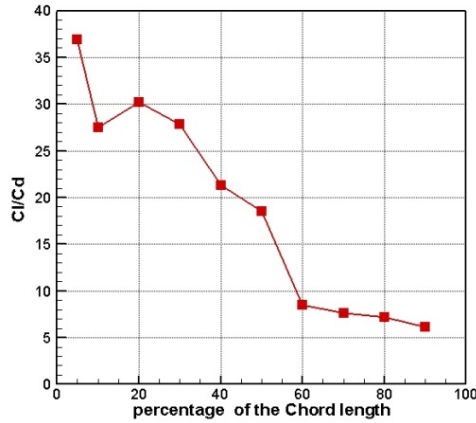


Fig. 14.  $\frac{C_l}{C_d}$  distributions with different second actuator location.

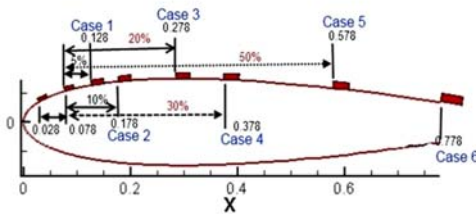


Fig. 15. Schematic of three actuators location.

Table 4 The mean lift and drag coefficients for different actuator locations

Case	Actuators location from leading edge	$C_l$	$C_d$	$\frac{C_l}{C_d}$
1	2.8%, 7.8% , 12.8% chord	1.7209	0.0684	25.1593
2	2.8%, 7.8% , 17.8% chord	1.6986	0.0687	24.7249
3	2.8%, 7.8% , 27.8% chord	1.7458	0.0573	30.4677
4	2.8%, 7.8% , 37.8% chord	1.7305	0.0557	31.0682
5	2.8%, 7.8% , 57.8% chord	1.7835	0.0772	23.1023
6	2.8%, 7.8% , 77.8% chord	1.7280	0.0844	20.4739

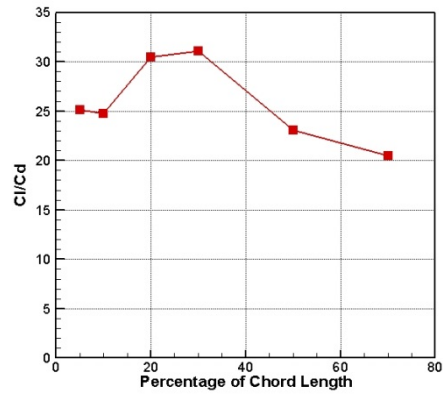


Fig. 16.  $\frac{C_l}{C_d}$  values with different second actuator location.

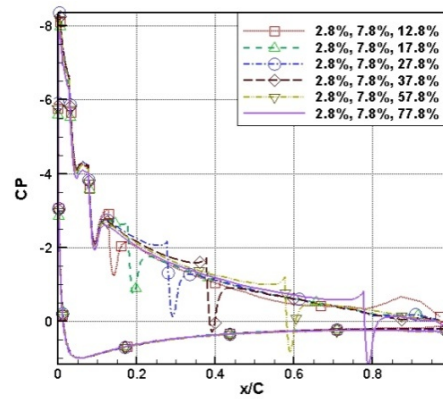


Fig. 17. Surface  $C_p$  distributions with three actuators in various locations,  $M=0.1$ , A.O.A. =15 deg.

Table 5 The mean lift coefficients ( $C_l$ )

Angle of Attack (degree)	The mean of lift coefficient			
	One Actuator	Two Actuators	Three Actuators	Four actuators
9	1.0306	0.9586	0.8248	0.8935
12	1.3621	1.6182	1.2847	1.5450
15	1.5195	1.7168	1.7209	1.5749
18	1.6885	1.9820	2.0136	1.8871
21	1.7322	1.7282	1.7581	2.1236
24	1.451	1.7326	1.6263	2.1295
27		1.5615	1.5403	2.1354
30		1.4208	1.5011	2.0950

#### 4. CONCLUSIONS

The effect of plasma body force on the flow field of stalled NACA 0015 airfoil at a Reynolds number of 45000 was simulated. Plasma body force was formed by the single and multiple DBD actuators in

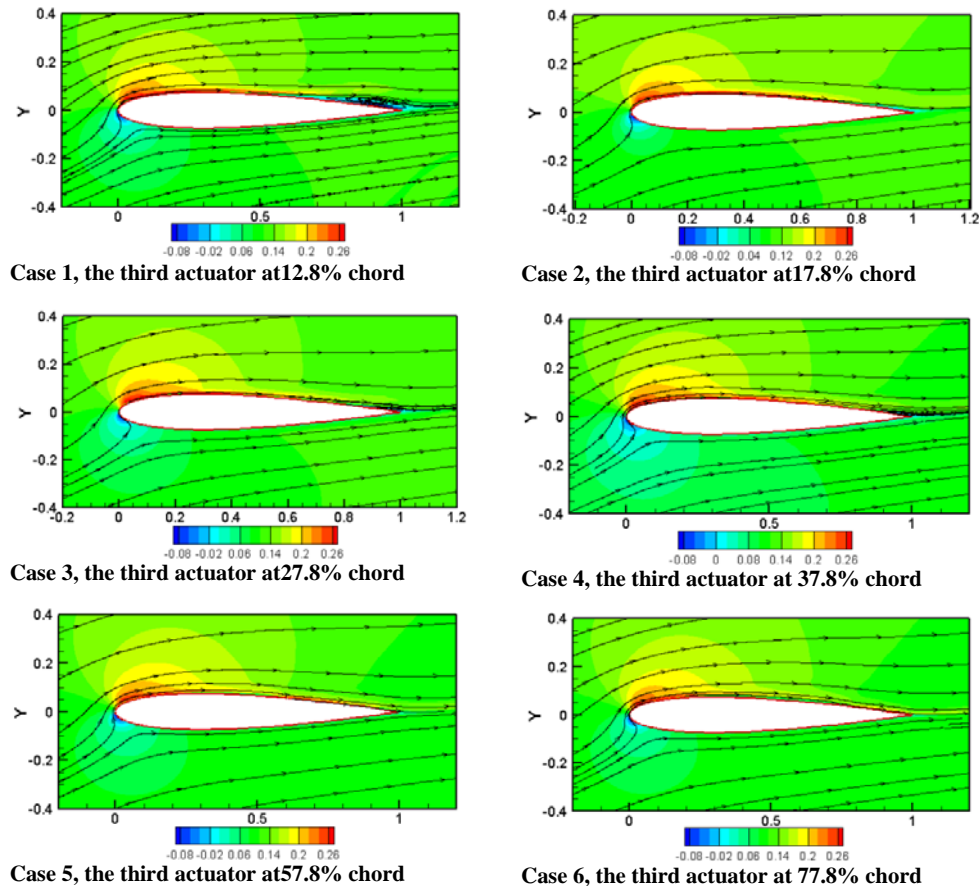


Fig. 18. Mean stream line and mean U-velocity contours from case1 to case 6.

steady mode. Two-dimensional unsteady compressible Navier-Stokes equations were employed together with Algebraic Prandtl turbulence modeling for simulation. The Shyy model was used to simulate the plasma body force. The responses of the separated flow field to single and multiple plasma actuators over a broad range of attack angles ( $9^\circ - 30^\circ$ ) were investigated. Also, the effects of the two and three plasma actuators' locations on the flow were studied. The results showed that multiple actuators have more impact on the flow separation control with the same electrical power requirements. It is suggested that in low angles of attack, one actuator gets used with maximum Dc. In medium angles of attack, two or three actuators are applied and in high angles of attack, four actuators are used for flow separation control. It seems that, if the DBD plasma actuators don't have interaction each other and input voltage greater than minimum voltage for ionized air surrounding actuator, by increasing number of actuators, the greater angles of attack can be controlled. Finally, the location of the actuators in multiple plasma actuators affects the performance coefficients and decreasing the distance between the first and second actuators improves the aerodynamic coefficients.

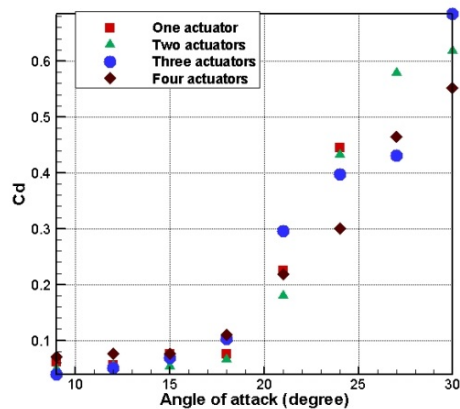


Fig. 19. Mean drag coefficients.

## REFERENCES

- Asada, K. and K. Fujii (2010). Computational Analysis of Unsteady Flow field Induced by Plasma Actuator in Burst Mode, *5th Flow Control Conference. AIAA 2010-5090. Chicago, Illinois.*
- Baird, C., C. Enloe, T. McLaughlin and J. Baughn (2005). Acoustic Testing of the dielectric

- barrier discharge (DBD) plasma actuator, *43rd AIAA Aerospace Sciences Meeting and Exhibit*, American Institute of Aeronautics and Astronautics.
- Corke, T., C. Enloe and S. Wilkinson (2010). Dielectric Barrier Discharge Plasma Actuators for Flow Control. *Annual Review of Fluid Mechanics* 42(1), 505–529.
- Corke, T. and M. Post (2005). Overview of Plasma Flow Control: Concepts, Optimization, and Applications, *43rd AIAA Aerospace Sciences Meeting and Exhibit*, American Institute of Aeronautics and Astronautics.
- Gaitonde, D. (2010). Three-dimensional plasma-based flow control simulations with high-fidelity coupled first-principles approaches, *International Journal of Computational Fluid Dynamics* 24(7), 259–279.
- Gaitonde, D., M. Visbal and S. Roy (2005). Control of Flow Past a Wing Section with Plasma-based Body Forces, *36th AIAA Plasmadynamics and Lasers Conference*, American Institute of Aeronautics and Astronautics.
- Greenblatt, D. and Wagnanski, I. J. (2000). The control of flow separation by periodic excitation, *Progress in Aerospace Sciences* 36(7), 487–545.
- Jahangirian, A. and M. Hadidoolabi (2005). Unstructured moving grids for implicit calculation of unsteady compressible viscous flows, *International Journal for Numerical Methods in Fluids* 47(10–11), 1107–1113.
- Jayaraman, B. and W. Shyy (2008). Modeling of dielectric barrier discharge-induced fluid dynamics and heat transfer *Progress in Aerospace Sciences* 44(3), 139–191.
- Jayaraman, B., Y. Lian and W. Shyy (2007). Low-Reynolds Number Flow Control Using Dielectric Barrier Discharge-Based Actuators, *37th AIAA Fluid Dynamics Conference and Exhibit*, American Institute of Aeronautics and Astronautics.
- Jayaraman, B. and W. Shyy (2003). Flow Control and Thermal Management Using Dielectric Glow Discharge Concepts, *33rd AIAA Fluid Dynamics Conference and Exhibit* 1-12.
- Jiangnan, H., T. Bali, W. Yulin, S. Yahui, P. Shucheng and L. Wenfeng (2014). Dielectric barrier plasma dynamics for active aerodynamic flow control. *Science China Physics, Mechanics and Astronomy* 57(2), 345–353.
- Kaneda, I., S. Sekimoto, T. Nonomura, K. Asada, A. Oyama and K. Fujii (2012). An Effective Three-Dimensional Layout of Actuation Body Force for Separation Control. *International Journal of Aerospace Engineering* 1–12.
- Kaneda, I. and K. Asada (2011). Effective Three dimensional Layout of Imaginary Body Force for Separation Control. *49th AIAA Aerospace Sciences Meeting and Exhibit* (January), Orlando, Florida.
- Khoshkhoo, R. and A. Jahangirian (2014). Flow Separation Control over Airfoils using DBD Plasma Body Force. *Journal of the Brazilian Society of Mechanical Sciences and Engineering*.
- Shyy, W., B. Jayaraman and A. Andersson (2002). Modeling of glow discharge-induced fluid dynamics. *Journal of Applied Physics* 92(11), 6434–6443.
- Tathiri, G., E. Esmaeilzadeh, S. M. Mirsajedi and H. M. Moghaddam (2014). Experimental Investigation of Why an AC Dielectric Barrier Discharge Plasma Actuator is Preferred to DC Corona Wind Actuator in Boundary Layer Flow Control. *Journal of Applied Fluid Mechanics* 7(3), 525–534.
- Tsubakino, D. and Y. Tanaka (2007). Effective Layout of Plasma Actuators for a Flow Separation Control on a Wing. *45th AIAA Aerospace Sciences Meeting and Exhibit*, Reno, Nevada.
- Visbal, M. R. (2010). Strategies for control of transitional and turbulent flows using plasma-based actuators. *International Journal of Computational Fluid Dynamics* 24(7), 237–258.
- Wilcox, C. D. (1998). *Turbulence modeling for CFD*, Second Edition, DCW Industries, California.